WEP Warwick Evans Publishing

Transactions on Engineering and Technology Research
ISSN: 2960-1797, eISSN: 2960-2246 | Volume 2
AMMEE 2024

Dynamic modeling and analysis of 3-RRCPR parallel pointing mechanism with clearance

Jing Sun [1], Jingwei Song [2], Yongjie Wang [3]

[1] College of Mechanical Engineering, North China University of Science and Technology, Tangshan, China

[2] College of Mechanical Engineering, Yanshan University, Qinhuangdao, China

[3] College of Mechanical Engineering, Yanshan University, Qinhuangdao, China

* Shihua Li

Abstract. In order to study the influence of kinematic pair clearance on the dynamic characteristics and pointing accuracy of 3-RRCPR parallel pointing mechanism, the dynamic model of spatial mechanism with three-dimensional revolute pair clearance is established. Firstly, the revolute pair mode considering three-dimensional clearance is established, and the normal and tangential contact force models between the kinematic pair elements are established based on Flores contact model and modified Coulomb friction model. Secondly, the dynamic model of parallel mechanism with clearance is established according to Lagrange multiplier method. Finally, the effects of different clearance sizes and loads on the dynamic characteristics and pointing accuracy of the mechanism are analyzed by numerical simulation. The results show that the increase of clearance size and load will reduce the pointing accuracy, and the decrease of clearance size and the increase of load will enhance the motion stability of the mechanism. Reasonable clearance and load matching is conducive to improving the accuracy of the mechanism. This study provides a theoretical basis for the study of the nonlinear dynamic characteristics and accuracy of the mechanism considering the clearance.

Keywords: Parallel mechanism; Clearance of the revolute pair; Dynamic model; Dynamic characteristics; Pointing accuracy

1. Introduction

The pointing mechanism is an important component of aerospace equipment such as space telescopes and spaceborne antenna radars, and its dynamic characteristics and pointing accuracy have a great impact on the working performance of aerospace equipment. The parallel mechanism is gradually used in the research and development of high-precision pointing mechanism due to its advantages of high stiffness and small motion error. In the pointing mechanism, there is a clearance between the kinematic pairs connecting two adjacent components, which will cause vibration and wear of the mechanism, and affect the positioning accuracy of the pointing mechanism. Therefore, it is necessary to consider the dynamic performance of the parallel pointing mechanism of the motion sub-clearance. It can provide a certain theoretical basis for the research and development of high-precision pointing mechanism. In recent years, domestic and foreign scholars have carried out a lot of research work on the dynamic behavior of mechanisms with clearances. Flores et al. [1] proposed a dynamic modeling and analysis method for a planar mechanism with multi-clearance kinematic pairs, and studied the influence changes of single-clearance and multi-clearance based on the crank-slider mechanism. Farahan et al. [2] studied the chaotic and periodic characteristics of a four-bar mechanism with a clearance under different crank angular velocity and clearance size. Huynh et al. [3] proposed a new double-slider linkage mechanism, and studied the influence of the clearance kinematic pair on the slider kinematic characteristics. Cavalieri et al. [4] proposed a new modeling method for the three-dimensional clearance revolute pair, and solved the dynamic equation of the space crank-slider mechanism by using the generalized -α integral method. Erkaya [5] studied the effect of joint clearance on the motion sensitivity of the manipulator, and proposed a dynamic neural network model

to evaluate the trajectory error of the end effector of the mechanism. Jian Zhang et al.[6]studied the influence of the clearance value and clearance position of the revolute pair on the dynamic response of the redundantly constrained planar four-bar linkage. Faxin Liu et al. [7,8] studied the effects of different clearance sizes and different revolute pair clearances on the dynamic performance of the crank-rocker type plug-and-drop mechanism. Bai et al. [9,10] studied the influence of the three-dimensional clearance of the revolute pair on the dynamic characteristics of the plane crank-slider mechanism and the space double-crank mechanism by constructing a revolute pair model with radial and axial clearances. Song et al. [11] constructed the dynamic equation of multi-clearance planar mechanism based on variational inequality and Hamiltonian principle, and studied the influence of multiple revolute pair clearances on crank-slider mechanism and multi-link mechanism.Varedi [12,13] studied the dynamic characteristics of a planar 3-RRR parallel mechanism with a clearance joint, and proposed a kinematics and dynamic optimization algorithm based on the link length and mass distribution to improve the performance of the mechanism with precision. Alok et al. [14] studied the influence of joint clearance on the kinematic performance of multi-loop planar mechanism through ADAMS simulation, and proposed a deviation quantification index to determine the clearance kinematic pair that has the greatest impact on the mechanism output. Wang Jian et al. [15,16] studied the change law of the output kinematic characteristics of the 3-CPARR parallel mechanism when the flexible branch contains a clearance kinematic pair. Cao Yi et al. [17,18] studied the influence of the revolute pair clearance on the dynamic behavior and chaotic characteristics of the 3-CPAR&R1R2 hybrid mechanism. Based on the newly proposed modified L-N contact force model, Hou et al. [19, 20] studied the influence of different parameter conditions on the chaotic phenomenon and impact characteristics of the RU-RPU two-rotation decoupled parallel mechanism with revolute pair clearance.

In view of the high-precision application requirements of pointing mechanisms, this paper establishes a dynamic modeling model for a 3-RRCPR parallel pointing mechanism considering its three-dimensional kinematic pair clearance, The influence law of the kinematic pair clearance on the mechanism accuracy is studied to provide a theoretical basis for improving the mechanism accuracy.

2. Structural analysis of 3-RRCPR parallel mechanism

The three-dimensional model of the 3-RRCPR parallel pointing mechanism is shown in Fig. 1 .The mechanism consists of three branch chains and moving and fixed platforms. It has 6 degrees of freedom. Compared with the series-parallel mechanism, the number of kinematic pairs of the new parallel mechanism is reduced, thereby reducing the number of constraints in the mechanism. It is beneficial to the dynamic modeling and analysis of the mechanism, and solves the static indeterminate problem of the series-parallel mechanism, and has higher motion accuracy and reliability.

Figure 1. 3-RRCPR parallel pointing mechanism model

Since the three branches of the 3-RRCPR parallel mechanism are exactly the same, to simplify the schematic diagram, only the first branch is used as an example to mark the position and direction of each coordinate system, as shown in Fig. 2 and Fig. 3. A fixed coordinate system o_P-$x_P y_P z_P$ is

established at the intersection of the axes of the revolute pairs A_1, A_2, and A_3; The x_p axis is parallel to the fixed platform and points to the secondary rotation center A_1 on the link 1. the z_p axis is perpendicular to the fixed platform, and the direction is upward; the y_p axis is directed by right hand rule is established. The moving coordinate system o_{13}-$x_{13}y_{13}z_{13}$ is established on the moving platform, o_{13} is the center of mass of the moving platform; the x_{13} axis is parallel to the moving platform and points to the revolute pair A_1 on the connecting rod 1, the initial moment is parallel to the x_p axis; the z_{13} axis moves the platform vertically, and the direction is upward, the direction of the y_{13} axis is determined by the right-hand rule.

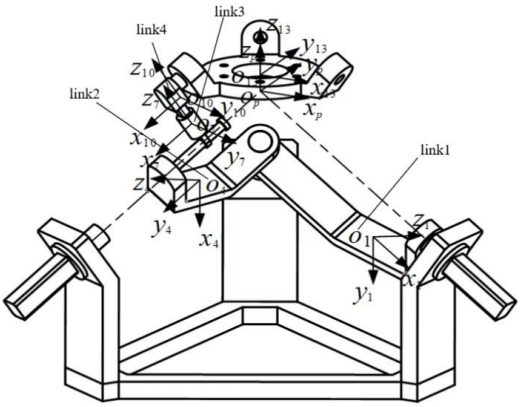

Figure 2. Schematic diagram of the establishment of the branch-chain coordinate system

A local coordinate system o_j-$x_jy_jz_j$ (j=1,2...12) is established at the centroid of each link of the three branch chains. The *x*-axis of the local coordinate system on each branch link 1 is parallel to the axis of the revolute pair A_i and points to the outside , the *y*-axis is parallel to the axis of the revolute pair B_i and points to the outside, and the *z*-axis direction is determined by the right-hand rule; The *x*-axis of the local coordinate system on each branch link 2 is parallel to the axis of the revolute pair B_i and points to the outside, the *y*-axis is parallel to the axis of the cylindrical pair C_i and points to the outside, and the *z*-axis direction is determined by the right-hand rule; The *x*-axis of the local coordinate system on the connecting link 3 is parallel to the axis of the cylinder pair C_i and points to the outside, the *z*-axis is along the axis of the connecting rod 3 and points upward, and the *y*-axis direction is determined by the right-hand rule; The *x*-axis of the local coordinate system on each branch link 4 is parallel to the axis of the revolute pair F_i and points to the outside, the *z*-axis is along the axis of the link 3 and points upward, the *y*-axis direction is determined by the right-hand rule, and the link local coordinate system on 4 is parallel to the axes of the local coordinate system on connecting rod 3. The poses of the moving coordinate system o_{13}-$x_{13}y_{13}z_{13}$ and the local coordinate system o_j-$x_jy_jz_j$ under the fixed coordinate system o_p-$x_py_pz_p$ can be expressed by ZYX Euler angles.

3. Dynamic modeling of 3-RRCPR mechanism with clearance

3.1. Description of the three-dimensional clearance revolute pair

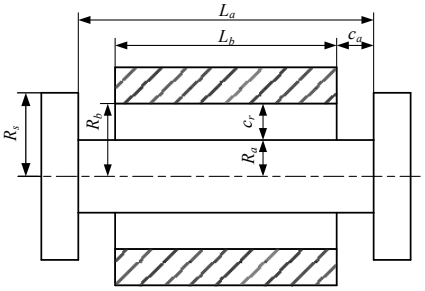

Figure 3. Model diagram of revolute pair clearance

Fig. 3 shows the geometric model of the revolute pair considering the clearance. There is not only a radial clearance but also an axial clearance between the rotating shaft and the shaft sleeve. Therefore, the rotating shaft can move radially and axially in the sleeve. This paper assumes that the axis of the rotating shaft and the axis of the sleeve are always parallel, that is, in the three-dimensional clearance revolute pair, the rotating shaft has four degrees of freedom of three-dimensional movement in the sleeve and rotation along the axis. The length of the rotating shaft is L_a, the radius is R_a, the length of the shaft sleeve is L_b, the radius of the inner cylindrical surface is R_b, and the radius of the end cover connected to the rotating shaft is R_s, then the axial clearance c_a and radial clearance c_r between the two are, respectively defined as:

$$c_a = \frac{L_a - L_b}{2}. \tag{1}$$

$$e = {}^{p}P_a - {}^{p}P_b. \tag{2}$$

As shown in Fig. 4, the radial collision model of the revolute pair is shown. P_a and P_b are the center points of the shaft and the sleeve respectively. The eccentricity vector $\boldsymbol{e}$ of the shaft and the sleeve in the Fig can be expressed as:

$$e = {}^{p}P_a - {}^{p}P_b. \tag{3}$$

Among them, ${}^{p}P_a$、${}^{p}P_b$represent the position coordinates of points P_a and P_b in the fixed coordinate system, respectively.

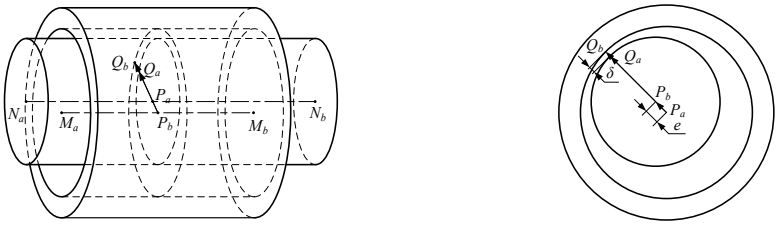

Figure 4. Radial collision model of revolute pair

The magnitude of the eccentricity $|\boldsymbol{e}|$ can be expressed as:

$$|e| = \sqrt{e^T e}. \tag{4}$$

The normal unit vector $\boldsymbol{n}_a$ of the contact point between the rotating shaft and the sleeve in the clearance revolute pair can be expressed as:

$$n_a = e/|e|. \tag{5}$$

The penetration depth δ_r when the shaft and the sleeve collide can be expressed as:

$$\delta_r = |e| - c_r. \tag{6}$$

Whether the revolute pair of the rotating shaft and the sleeve are in contact in the radial direction can be judged by Eq. 6. when $\delta_r < 0$, there is no contact and the rotating shaft moves freely in the sleeve. When $\delta_r = 0$,the rotating shaft and the sleeve begin to contact or begin to separate. when $\delta_r > 0$, the rotating shaft and the sleeve come into contact and deform.

When a collision occurs, the position vectors ${}^{p}Q_a$ and ${}^{p}Q_b$ of the corresponding contact points on the rotating shaft and the shaft sleeve in the fixed coordinate system can be expressed as:

$$ {}^{p}Q_a = r_{o10} + T_{10}\,{}^{10}P_a + R_a n_a. \tag{7} $$

$$ {}^{p}Q_b = r_{o13} + T_{13}\,{}^{13}P_b + R_b n_a. \tag{8} $$

Among them, ${}^{10}\boldsymbol{P}_a$ is the position vector of the point P_a in the local coordinate system o_{10}-$x_{10}y_{10}z_{10}$; ${}^{13}\boldsymbol{P}_b$ is the position vector of the point P_b in the moving coordinate system o_{13}-$x_{13}y_{13}z_{13}$.
By calculating the derivative with respect to time on both sides of Eq. 7 and Eq. 8, the velocity of the contact point in the fixed coordinate system can be obtained as:

$$ {}^{\dot{p}}Q_a = \dot{r}_{o10} + \dot{T}_{10}\,{}^{10}P_a + R_a \dot{n}_a. \tag{9} $$

$$ {}^{\dot{p}}Q_b = \dot{r}_{o13} + \dot{T}_{13}\,{}^{13}P_b + R_b \dot{n}_a. \tag{10} $$

Then the relative contact collision velocity can be expressed as:

$$ \dot{\delta}_r = {}^{\dot{p}}Q_a - {}^{\dot{p}}Q_b. \tag{11} $$

By projecting the relative velocities of the contact points to the normal and tangential directions, respectively, the normal and tangential collision velocities $\boldsymbol{v}_{na}$ and $\boldsymbol{v}_{ta}$ can be obtained as:

$$ v_{na} = \dot{\delta}_r^{\,T} n_a \cdot n_a. \tag{12} $$

$$ v_{ta} = \dot{\delta}_r - v_{na} = |v_{ta}|\tau_a. \tag{13} $$

$\boldsymbol{\tau}_a$ represents the tangent direction of the contact surface of the clearance kinematic pair, which can be expressed as:

$$ \tau_a = v_{ta}/|v_{ta}|. \tag{14} $$

The axial collision model of the revolute pair is shown in Fig. 5. M_a and M_b are the center points of the upper end faces of the shaft sleeve, N_a and N_b are the center points of the two inner end faces of the shaft, F_a is the midpoint of the shaft sleeve axis, and the shaft axis is parallel to the axis of the sleeve. The contact form between the shaft and the shaft sleeve in the axial direction is surface contact. The center points M_a and M_b of the two end faces of the shaft sleeve are equivalent to the contact collision points on the shaft sleeve, then the axis of the shaft sleeve and the two inner end faces of the shaft. H_b is the contact collision point on the rotating shaft.

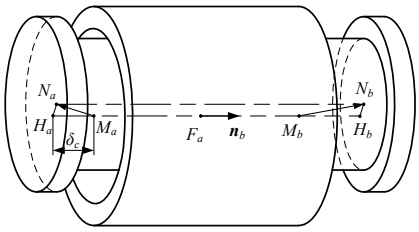

Figure 5. Axial collision model of revolute pair

The position vector of the contact collision point M_a on the sleeve can be expressed as:

$$^{p}M_a = r_{o13} + T_{13}\,{}^{13}M_a. \tag{15}$$

Among them, represents the position vector of the point M_a in the moving coordinate system o_{13}-$x_{13}y_{13}z_{13}$.

The normal unit vector $\boldsymbol{n}_b$ of the axial collision can be expressed as:

$$n_b = \frac{\overrightarrow{M_aM_b}}{|\overrightarrow{M_aM_b}|}. \tag{16}$$

The penetration depth δ_c at the collision point M_a can be expressed as:

$$\delta_c = \left(\overrightarrow{M_aN_a}\right)^T n_b. \tag{17}$$

According to Eq. 17, it can be judged that when$\delta_c < 0$ there is no axial collision between the shaft and the sleeve, When$\delta_c = 0$, the shaft and the sleeve begin to contact or separate in the axial direction, and when$\delta_c > 0$, an axial collision occurs between the shaft and the sleeve.

The position vector of the contact collision point H_a on the rotating shaft in the fixed coordinate system is:

$$^{p}H_a = {}^{p}M_a + \delta_c n_b. \tag{18}$$

By taking the derivative of Eq. 18 with respect to time, the velocity of the collision point H_a in the fixed coordinate system can be obtained as:

$$^{p}\dot{H}_a = {}^{p}\dot{M}_a + \dot{\delta}_c n_b + \delta_c \dot{n}_b. \tag{19}$$

The velocity vector of the collision point M_a in the fixed coordinate system is:

$$^{p}\dot{M}_a = \dot{r}_{o13} + \dot{T}_{13}\,{}^{13}M_a. \tag{20}$$

According to Eq. 19 and Eq. 20, the contact speed between the shaft and the sleeve can be expressed as:

$$\dot{\delta}_c = {}^{p}\dot{H}_a - {}^{p}\dot{M}_a. \tag{21}$$

Projecting the contact velocity at the collision point M_a to the normal direction $\boldsymbol{n}_b$, the normal contact velocity can be obtained as:

$$v_{nb} = \dot{\delta}_c^{\ T} n_b. \tag{22}$$

Then the tangential contact velocity can be expressed as:

$$v_{tb} = \dot{\delta}_c - v_{nb}. \tag{23}$$

The tangential unit vector at the collision point can be expressed as:

$$\tau_b = v_{tb}/|v_{tb}|. \tag{24}$$

As shown in Fig. 5, the contact collision model at the collision points M_b and H_b is similar to that of the M_a and H_a points, and can be obtained in the same way.

3.2. Establishment of contact force model

Among the many collision models, the Flores contact force model, compared with the L-N contact force model, takes into account the elastic deformation and damping of the contact surface after the contact of the kinematic pair elements, and is not restricted by the coefficient of restitution. It is widely used in the dynamic calculation of mechanisms with clearances. Therefore, this chapter uses the Flores contact force model to calculate the contact force in the radial collision direction of the clearance kinematic pair. The normal contact force F_{nr} expressed based on the Flores contact force model is:

$$F_{nr} = K_r \delta_s^n [1 + \frac{8(1-c_e)}{5c_e} \frac{\dot{\delta}_s}{\dot{\delta}_s^{(-)}}]. \tag{25}$$

Among them, K_r represents the contact stiffness coefficient, which is related to the geometry of the contact surface and the material properties; c_e is the coefficient of restitution, and its value is related to the material properties. The coefficient of restitution of hard materials is larger, and the coefficient of restitution of soft materials is smaller; n is the force index, which is set to 1.5; δ_s represents the penetration depth of the contact collision surface; $\dot{\delta}_s$ is relative contact velocity of the contact point, and its value is the derivative of δ_s in the formula; $\dot{\delta}_s^{(-)}$ is the initial collision velocity, which is generally artificially given according to the specific mechanism of the study, but it is stipulated that the initial contact velocity should be lower than the propagation velocity of the collision elastic wave in the contact body, that is, the initial contact velocity should satisfy:

$$\dot{\delta}_s^{(-)} \leq 10^{-5} \sqrt{E_s/\rho}. \tag{26}$$

Among them, ρ is the material density of the contacting member; E_s is the comprehensive elastic modulus of the contacting member, expressed as:

$$\frac{1}{E_s} = \frac{1-\upsilon_a^2}{E_a} + \frac{1-\upsilon_b^2}{E_b}. \tag{27}$$

υ_a and υ_b represent the Poisson's ratio of the contact members a and b respectively, and E_a and E_b are the elastic moduli of the contact members a and b, respectively.

The contact stiffness coefficient K_r in Eq. 3- Eq. 25 can be expressed as:

$$K_r = \frac{4E_s}{3}\sqrt{\frac{R_a R_b}{R_b - R_a}}. \tag{28}$$

In this paper, the modified Coulomb friction model is used to solve the tangential contact force of the clearance pair. The model avoids the sudden change of the tangential contact force when the speed is small by setting the speed limit. It meets the actual situation that the tangential contact force is zero when the tangential contact velocity of the contact surface is extremely small, thereby improving the stability of the integral solution of the dynamic differential equation. The tangential contact force of the rotating shaft to the sleeve can be expressed as:

$$F_{\tau r} = c_f c_d F_{nr}. \tag{29}$$

Among them, c_f is the sliding friction coefficient; c_d is the dynamic correction coefficient, which satisfies the relationship:

$$c_d = \begin{cases} 0 |v_t| < v_s \\ \frac{|v_t| - v_s}{v_d - v_s} v_s \le |v_t| \le v_d \\ 1 v_d < |v_t| \end{cases}. \tag{30}$$

Among them, $\boldsymbol{v_s}$ and $\boldsymbol{v_d}$ are the given speed values used to divide the variation interval of the correction coefficient c_d.

For the axial contact, that is, the contact between the plane and the plane, the linear model is used to calculate the normal contact collision force, which can be expressed as:

$$F_{nc} = K_c \delta_c. \tag{31}$$

Among them, K_c is the contact stiffness coefficient of the axial collision, which can be expressed as:

$$K_c = \frac{R_s - R_b}{0.475} E_s. \tag{32}$$

The modified Coulomb friction model is still used for the tangential contact force model of the axial collision of the clearance revolute pair.

Through the contact force model, the total collision force vector of the shaft to the sleeve can be obtained as:

$$F_b = [F_{xb} \quad F_{yb} \quad F_{zb}]^T = F_r + F_c. \tag{33}$$

Among them, $\boldsymbol{F_{xb}}$、$\boldsymbol{F_{yb}}$、$\boldsymbol{F_{zb}}$ are the components of the collision force of the rotating shaft on the shaft sleeve in the x_p, y_p and z_p directions in the fixed coordinate system respectively; $\boldsymbol{F_r}$, $\boldsymbol{F_c}$ are the radial and axial contact force vectors, respectively.

According to the acting force and the acting reaction force, it can be known that the collision force of the shaft sleeve on the rotating shaft is expressed as:

$$F_a = -F_b. \tag{34}$$

From the contact force model, the collision forces of the three potential contact points on the bush in the three-dimensional revolute pair clearance model are obtained as $\boldsymbol{F_{Qb}}$, $\boldsymbol{F_{Ma}}$, $\boldsymbol{F_{Mb}}$, respectively, Then

the moment generated by the collision force at the clearance to the center of mass of the upper moving platform of the branch chain of the 3-RRCPR mechanism is:

$$M_{Qb} = \left({}^{p}Q_b - r_{o13} \right) \times F_{Qb}. \tag{35}$$

$$M_{Ma} = \left({}^{p}M_a - r_{o13} \right) \times F_{Ma}. \tag{36}$$

$$M_{Mb} = \left({}^{p}M_b - r_{o13} \right) \times F_{Mb}. \tag{37}$$

3.3. Dynamic Modeling with Clearance

The position constraint equations and driving constraint equations of the 3-RRCPR parallel pointing mechanism are established, and the kinematic constraint equation of the revolute pair with clearance is obtained as:

$$\Phi_{rc}(q,t) = \left[\Phi^{r}(q,t), \Phi_j^{p}(q,t), \Phi_j^{s}(q,t) \right]^{T} = 0. \tag{38}$$

Among, $\Phi^{r}(q,t)$ is the constraint equation of the revolute pair at A_j, B_j, E_2, E_3 on each branch chain, $\Phi^{c}(q,t)$is the constraint equation of the cylinder pair at D_j, $\Phi^{p}(q,t)$ is the constraint equation of the moving pair at E_j, $\Phi^{d}(q,t)$ is the driving constraint equation.
The velocity constraint equation can be obtained by taking the first derivative with respect to time of Eq. 38:

$$\Phi_{rcq}\dot{q} = -\Phi_{rct}. \tag{39}$$

The acceleration constraint equation can be obtained by taking the second derivative with respect to time of Eq. 38:

$$\Phi_{rcq}\ddot{q} = -\left(\Phi_{rcq}\dot{q}\right)_q \dot{q} - 2\Phi_{rcqt}\dot{q} - \Phi_{rctt} \equiv \gamma_{rc}. \tag{40}$$

The dynamic formulas of the system with clearances with Lagrange multipliers are established as follows:

$$\begin{bmatrix} M & \Phi_{rcq}{}^{T} \\ \Phi_{rcq} & 0 \end{bmatrix} \begin{bmatrix} \ddot{q} \\ \lambda \end{bmatrix} = \begin{bmatrix} Q_{rc} \\ \gamma'_{rc} \end{bmatrix}. \tag{41}$$

$\boldsymbol{Q}_{rc}$ is the generalized force vector including the contact force; $\gamma'_{rc}$is acceleration terms constructed using Baumgarte's default stabilization algorithm can be represented as:

$$Q_{rc} = Q_{ex} + F_{tol} + M_{tol}. \tag{42}$$

$$\gamma'_{rc} = \gamma_{rc} - 2\alpha_{rc}\dot{\Phi}_{rc} - \beta_{rc}^{2}\Phi_{rc}. \tag{43}$$

Among them, $\boldsymbol{F}_{tol}$ and $\boldsymbol{M}_{tol}$ represent the resultant force of the contact force and moment acting on the shaft and the shaft sleeve respectively.

4. Numerical simulation

In this paper, the fourth-order Runge-Kutta method is used to solve the dynamic model of the 3-RRCPR parallel pointing mechanism with three-dimensional revolute pair clearance. The

dimensional parameters and mechanical parameters of each component of the 3-RRCPR parallel mechanism can be measured by Solidworks software. When calculating the tangential contact force, the speed extremes v_s and v_d are 0.1mm/s and 1mm/s, respectively. Setting the elastic moduli E_a and E_b of the rotating shaft and the shaft sleeve to 7.2×10^4Mpa, the Poisson's ratio υ_a and υ_b to be 0.33, the recovery coefficient c_e to be 0.9, the sliding friction coefficient c_f to be 0.03, and the correction parameters α_s and β_s to be 40 and 50, respectively. The simulation integration step size is 1×10^{-4}s.

Given the motion trajectory of the center of mass of the 3-RRCPR Parallel mechanism motion platform. By calculating the inverse kinematics solution of the 3-RRCPR mechanism through Matlab, the driving angular displacements of the revolute pairs A_1, A_2, and A_3 and the driving displacements of the moving pairs E_1, E_2, and E_3 can be obtained. The motion trajectory of the center of mass of the moving platform is:

$$\begin{cases} \psi_{13} = 2\pi\, sin(\pi t) \\ \theta_{13} = \frac{\pi}{6} sin(\pi t) \\ \varphi_{13} = -2\pi\, sin(\pi t) \end{cases} . \tag{44}$$

$$\begin{cases} x_{13} = z_0\, sin(\theta_{13})\, cos(\psi_{13}) \\ y_{13} = z_0\, sin(\theta_{13})\, sin(\psi_{13}) \\ z_{13} = z_0\, cos(\theta_{13}) + 5\, sin(\pi t) \end{cases} . \tag{45}$$

ψ_{13}、θ_{13}、φ_{13} are the azimuth angle, pitch angle and rotation angle of the moving platform respectively; z_0 is the distance from the origin o_{13} of the moving coordinate system to the origin o_p of the fixed coordinate system at the initial moment.

The load of the moving platform of the mechanism and the size of the clearance of the revolute pair are important factors that affect the dynamic performance and pointing accuracy of the mechanism. In this paper, numerical simulations are carried out under three clearance sizes (0.1mm, 0.2mm, 0.3mm) and three loads (0kg, 250kg, 500kg). The effects of different clearance sizes and load conditions on the dynamic characteristics of the parallel mechanism were compared and analyzed.

According to the dynamic model of the 3-RRCPR mechanism with clearance, the dynamic response of the mechanism under different clearances was numerically solved by using Matlab software. The displacement and acceleration curves of the center of mass of the moving platform of the mechanism under different clearances can be calculated as shown in Fig. 6.

It can be seen from Fig. 6(f) that when the kinematic pair clearance increases, the displacement curve of the center of mass of the moving platform of the 3-RRCPR mechanism deviates from the ideal curve, and the larger the clearance value, the higher the degree of deviation. For the angular displacement of the 3-RRCPR mechanism, the curves under different clearance values basically coincide with the curves under ideal conditions, indicating that the existence of the kinematic pair clearance has a great influence on the linear displacement of the moving platform but has little effect on the angular displacement. It can be seen from Fig. 6(l) that when the clearance increases, the fluctuation peak value of the linear acceleration of the moving platform increases significantly, especially the acceleration changes in the Y direction are more severe. The angular acceleration of the moving platform in three directions also has a certain degree of sudden change, but when the clearance increases, the fluctuation peak value of angular acceleration has no obvious change rule. At 0.4s, the peak value of the angular acceleration curve with a clearance of 0.2mm is larger, indicating that the joint clearance will cause fluctuations in the angular acceleration of the moving platform, but the impact is small. It is consistent with the change of the angular displacement and angular velocity curve.

Considering that the loads of the 3-RRCPR parallel pointing mechanism are 0kg, 250kg, and 500kg,

respectively, the dynamic response changes of the 3-RRCPR parallel pointing mechanism are studied. The dynamic response curves of the 3-RRCPR parallel pointing mechanism under different load conditions are shown in Fig. 7.

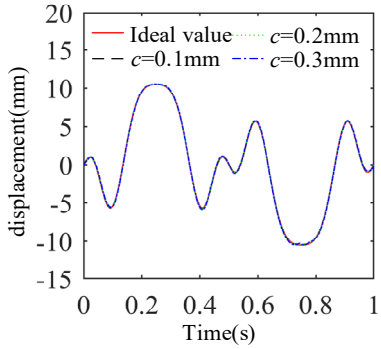

a) Displacement curve in X direction

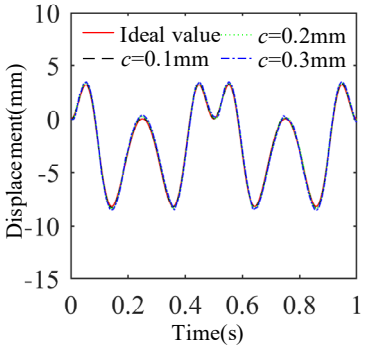

b) Displacement curve in Y direction

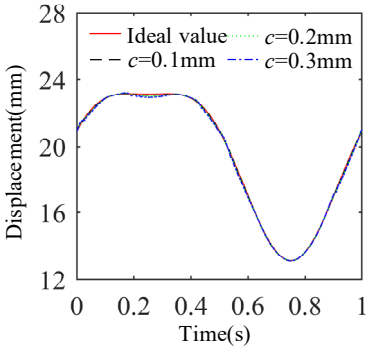

c) Displacement in Z direction

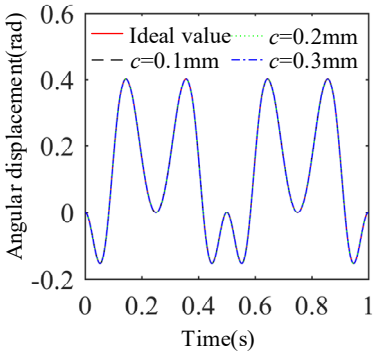

d) Angular displacement of Euler angle α

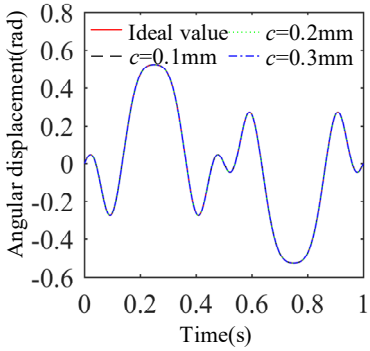

e) angular displacement of Euler angle β

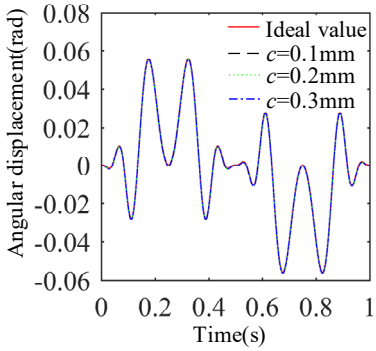

f) angular displacement of Euler angle γ

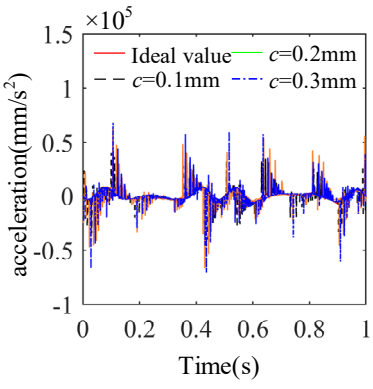

g) X-direction acceleration curve

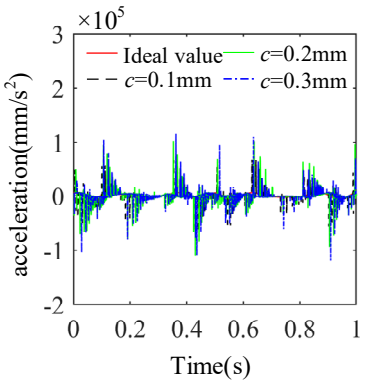

h) Y-direction acceleration curve

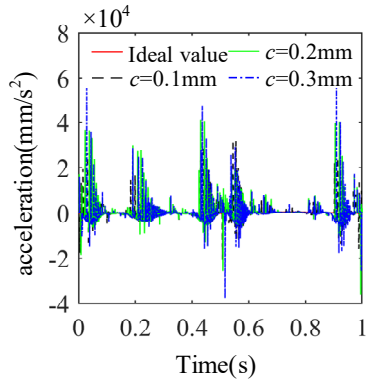

i) Z direction acceleration

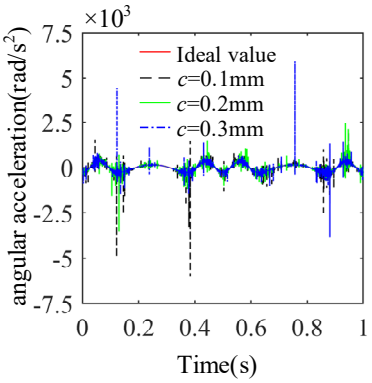

j) angular acceleration of Euler angle α

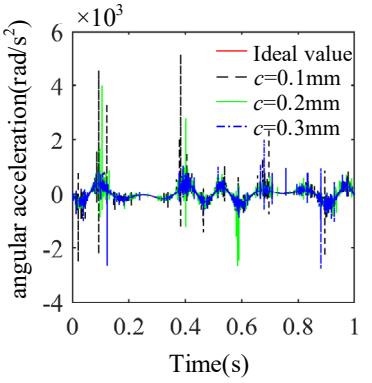

k) angular acceleration of Euler angle β

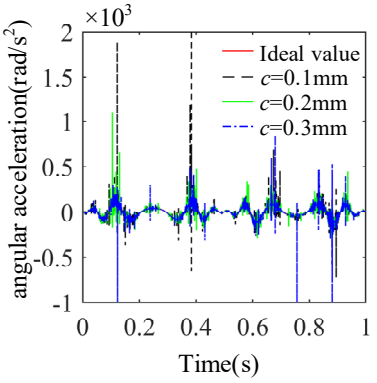

l) angular acceleration of Euler angle γ

Figure 6. Mechanism dynamics response curve under different clearances

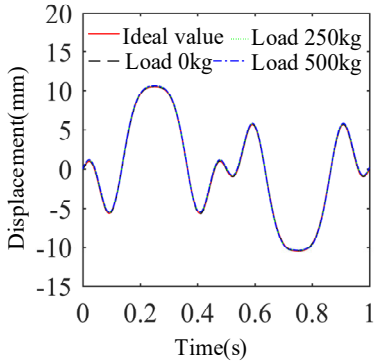

a) Displacement curve in X direction

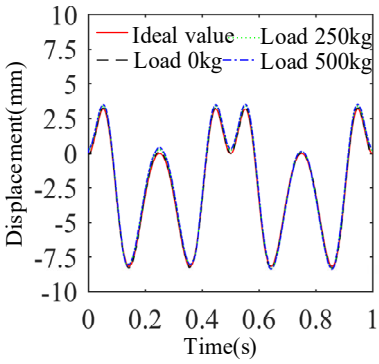

b) Displacement curve in Y direction

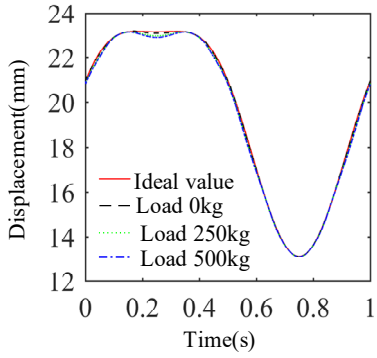

c) Displacement in Z direction

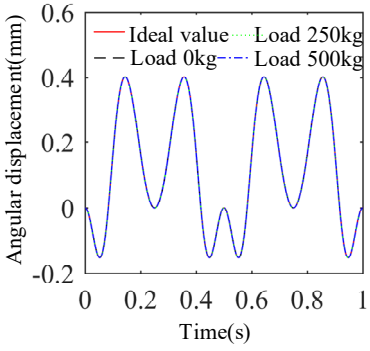

d) Angular displacement of Euler angle α

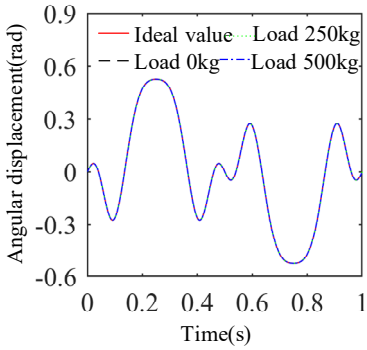

e) angular displacement of Euler angle β

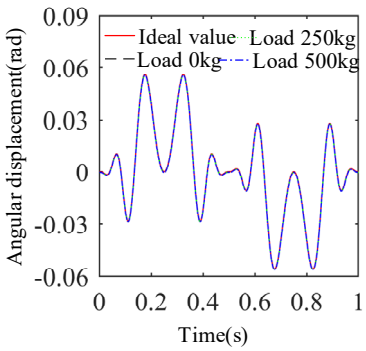

f) angular displacement of Euler angle γ

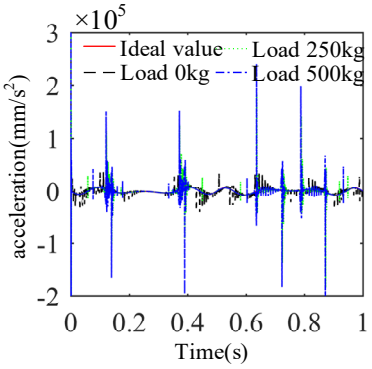

g) X-direction acceleration curve

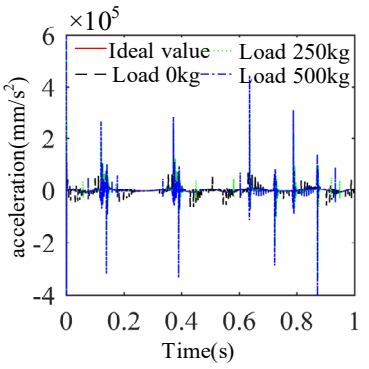

h) Y-direction acceleration curve

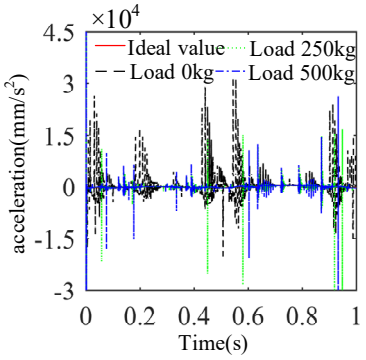

i) Z direction acceleration

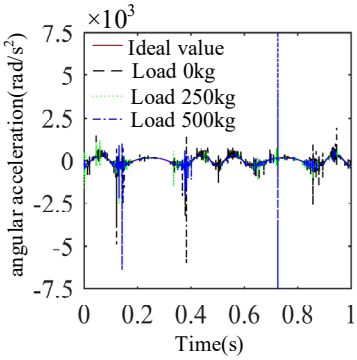

j) angular acceleration of Euler angle α

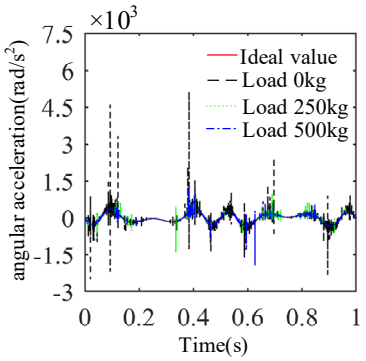

k) angular acceleration of Euler angle β

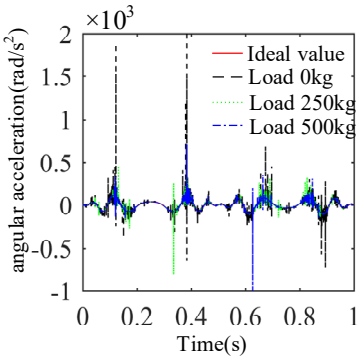

l) angular acceleration of Euler angle γ

Figure 7. Dynamic response curve of mechanism under different loads

It can be seen from Fig.7(f) that when the load of the moving platform increases, the displacement curve of the center of mass of the moving platform of the 3-RRCPR mechanism deviates from the curve under ideal conditions, and the larger the load value, the greater the deviation. Among them, the X-direction displacement does not change significantly, and the Y-direction displacement has a large deviation at the peak, while the Z-direction displacement has a large deviation at 0.25s, and the change is small at other times. The angular displacement curve of the 3-RRCPR mechanism is basically consistent with the ideal curve under different load conditions, indicating that the load has

a great influence on the linear displacement of the moving platform but little on the angular displacement. From Fig. 7(l), when the load increases, the peak value of the linear acceleration of the moving platform increases significantly, and it can be clearly seen that when the load is 500kg, the time interval of the first four sudden changes of the acceleration curve is approximately 0.02s, the interval of the last four sudden changes is 0.09s, which indicates that the driving function of the mechanism also has a certain influence on the change of the acceleration of the mechanism. The peak value of angular acceleration fluctuation of 3-RRCPR mechanism has no obvious change law. When the load increases, the angular acceleration curve does not show a huge fluctuation similar to the linear acceleration curve. It shows that the change of load has little influence on the rotational motion of the mechanism.

5. Conclusion and Innovation

(1) Innovation: A mathematical model to describe the three-dimensional clearance of the revolute pair is constructed, and the position vectors and contact judgment conditions of the three potential contact points of the revolute pair with the clearance are given.

(2) The Flores model and the improved Coulomb friction model are used to complete the construction of the contact force model of the three-dimensional clearance revolute pair. Combining the ideal dynamic equation of the 3-RRCPR parallel mechanism with the clearance model and the contact force model, the dynamic model of the parallel mechanism considering the three-dimensional clearance of the revolute pair is obtained. This dynamic modeling method can also be used in other space mechanisms.

(3) Through the analysis of the dynamic characteristics of the 3-RRCPR parallel mechanism under different clearance sizes and moving platform loads, it can be known that reducing the size of the clearance and increasing the load is conducive to enhancing the stability of the movement of the mechanism. Reasonable clearance and load matching are conducive to improving the accuracy of the mechanism.

Acknowledgements

We would like to thank the financial support from Theoretical Research on Precision Design of Weakly Coupled Flexible Secondary Mirror Adjustment Mechanism of Space Telescope (52275032) of National Natural Science Foundation of China (Surface Project); Key Project of Natural Science Foundation of Hebei Province Research on Design Theory of High-precision Shaft Coupled Fatigue Durability Test Platform(E2022203077); Basic scientific research expenses of colleges and universities in Hebei Province(JQN2023027).

References

[1] P. Flores, H M. Lankarani. Journal of Computational and Nonlinear Dynamics Dynamic Response of Multibody Systems with Multiple Clearance Joints[J]. 7(3): 031003. (2012)

[2] S B. Farahan, M R. Ghazavi, S. Rahmanian. Nonlinear Dynamics, Bifurcation in A Planar Four-Bar Mechanism with Revolute Clearance Joint[J]. 87(2): 955-973. (2017)

[3] N T. Huynh, S C. Huang, T P. Dao. Sadhana. Design Variables Optimization Effects on Acceleration and Contact Force of The Double Sliders-Crank Mechanism Having Multiple Revolute Clearance Joints by Use of The Taguchi Method Based on A Grey Relational Analysis[J]. 45(1), 1-22. (2020)

[4] S. Erkaya. Journal of Mechanical Engineering, Effects of Joint Clearance on The Motion Accuracy of Robotic Manipulators[J], 64(2): 82-94. (2018)

[5] F J. Cavalieri, A. Cardona. Mechanism and Machine Theory, Non-Smooth Model of A Frictionless and Dry Three-Dimensional Revolute Joint with Clearance for Multibody System Dynamics[J]. 121: 335-354. (2018)

[6] Jian Zhang, Haidong Yu, Lin LI, et al. Machine Design & Research. Dynamic performance analysis for over-constrained mechanisms with multiple revolute clearance joints[J]. 34(1): 76-81+86. (2018)

[7] Faxin Liu, Chuanyu Wu, Liang Sun. Transactions of the Chinese Society of Agricultural Engineering. Analysis and test of influence of revolute joint clearance on performance of crank-rocker style transplanting mechanism[J]. 32(15): 9-17. (2016)

[8] Lixin Xu, Yonggang LI, Chongning LI, Yuhu Yang. Journal of Mechanical Engineering. Analysis of the influence of bearing clearance and flexible characteristics on mechanism dynamic error[J]. 48(07):30-36. (2012)

[9] Z F. Bai, X. Jiang, J Y. Li, et al. Journal of Vibration and Control.Dynamic. Analysis of Mechanical System Considering Radial and Axial Clearances in 3D Revolute Clearance Joints[J]. 27(15): 1893-1909. (2020)

[10] Xupeng Wang;Geng Liu;Shangjun Ma;Ruiting Tong . Journal of Sound and Vibration .Study on dynamic responses of planar multibody systems with dry revolute clearance joint: Numerical and experimental approaches[J]. 2019

[11] N Song, H J Peng, X M Xu, et al. Mechanism and Machine Theory,Modeling and Simulation of A Planar Rigid Multibody System with Multiple Revolute Clearance Joints Based on Variational Inequality[J]. 154: 1-22. (2020)

[12] S M. Varedi K, M. Daniali H, M. Farajtabar. Robotica The Effects of Joint Clearance on The Dynamics of The 3RRR Planar Parallel Manipulator[J]. 35(6): 1223-1242. (2016)

[13] K S M. Varedi, H M. Daniali, M. Farajtabar, et al. Nonlinear Dynamics. Reducing The Undesirable Effects of Joints Clearance on The Behavior of The Planar 3-RRR Parallel Manipulators[J]. 86(2): 1007-1022. (2016)

[14] S. Alok, K. Chaudhary, A. Guha. Sadhana. A Study on Critical Order of Joints with Clearances and Its Effect on Kinematic Performance of Multiloop Planar Mechanisms[J]. 45(1): 1-12. (2020)

[15] Jian Wang, Hu Dong, Zhaodong Wang, et al. Journal of Vibration and Shock. Elastic dynamic modeling and analysis for a 3-CPaRR decoupled parallel mechanism with joint clearance [J]. 39(5): 118-130. (2020)

[16] Gengxiang Wang, Hongzhao Liu. Journal of Mechanical Engineering.Dynamic analysis of 4-SPS/CU parallel mechanism considering spherical sub-clearance[J]. 51(01):43-51. (2015)

[17] Yi Cao, Junchen Liu, Minghao Zhai, et al. Journal of Huazhong University of Science and Technology(Natural Science Edition).Dynamics analysis of 3-CPaR&R1R2 hybrid mechanism with joint clearance[J]. 47(12): 48-54. (2019)

[18] Jingyuan Zhu, Jian Wang, Zehua Ding, Hui Zhou, Yi Cao. Vibration and shock. Kinematic and dynamic analysis of 3-CP_aRR parallel mechanism with joint space[J]. 37(18):9-17+29. (2018)

[19] Yulei Hou, Guoning Jing, Yunjiao Deng et al. China Mechanical Engineering,Dynamics modeling and characteristics analysis of a two rotational parallel mechanism with revolute joint clearances[J]. 29(2): 158-165. (2018)

[20] Yulei Hou, Yi Wang, Guoning Jing, et al. Journal of Vibration and Shock,Chaos and impact phenomena of a RU-RPR decoupled parallel mechanism containing clearance[J]. 36(1): 215-222+239.(2017)